Journal of Materials Processing Technology 211 (2011) 503–512

Contents lists available at ScienceDirect

Journal of Materials Processing Technology

journal homepage: www.elsevier.com/locate/jmatprotec

Performance of activated TIG process in austenitic stainless steel welds

Kuang-Hung Tseng*, Chih-Yu Hsu

Department of Materials Engineering, National Pingtung University of Science and Technology, 1, Hseuhfu Rd., Neipu, Pingtung 912, Taiwan

ARTICLE INFO

Article history:
Received 31 May 2010
Received in revised form 11 October 2010
Accepted 11 November 2010

Keywords:
Welding
Stainless steel
Weld morphology
Angular distortion
Oxide flux

ABSTRACT

Five kinds of oxide fluxes, MnO_2, TiO_2, MoO_3, SiO_2, and Al_2O_3, were used to investigate the effect of activated tungsten inert gas (activated TIG) process on weld morphology, angular distortion, delta-ferrite content, and hardness of Type 316L stainless steels. An autogenous TIG welding was applied to 6 mm thick stainless steel plates through a thin layer of flux to produce a bead-on-plate welded joint. The oxide fluxes used were packed in powdered form. The experimental results indicated that the SiO_2 flux facilitated root pass joint penetration, but Al_2O_3 flux led to the deterioration in the weld depth and bead width compared with conventional TIG process. Activated TIG welding can increase the joint penetration and weld depth-to-width ratio, thereby reducing angular distortion of the weldment. On the basis of the present results, it is considered that the centripetal Marangoni convection and constricted arc plasma as a mechanism in increasing the penetration of activated TIG joint.

1. Introduction

Traditional austenitic stainless steels, such as the Type 300 series, contain sufficient amounts of chromium to guarantee corrosion resistance, along with nickel to ensure the austenite phase at room temperature. The basic composition of traditional austenitic stainless steel includes 18% chromium and 8% nickel alloy, but can also include alloys of molybdenum, titanium, niobium, copper, and nitrogen. Because of their excellent corrosion resistance, better creep rupture strength at high temperature, and impact resistance at low temperatures, austenitic stainless steels are often used in industrial plants, chemical processing, food production, marine hardware, furnaces, heat exchangers, gas turbines, and cryogenic vessels. Tseng and Chou (2001, 2002a, 2002b) reported that an austenitic stainless steel exhibits considerably higher thermal expansion than other stainless steels, and the thermal conductivity is generally lower than that of carbon steel. Such characteristics cause a serious thermal stress in applications with temperature fluctuations, heat treatment of complete structures, and on welding.

During welding, the arc heats a joint plate is locally, and the temperature distributions in the weldment are not uniform. Heating and cooling cycles induce non-uniform thermal strains in both the weld metal and the adjacent base metal. The thermal strains produced during heating then produce plastic upsetting. These non-uniform thermal stresses combine and react to produce internal forces that cause shrinkage and distortion. Tseng and Chou (2003) showed a presence of the shrinkage and distortion in turn affects the fabrication, precision (shape and dimensional tolerance), and function (reliability and stability) of finished products.

Gas tungsten arc welding, also known as tungsten inert gas (TIG) welding, produces an arc between a tungsten electrode and the workpiece. An inert gas shields the arc, electrode, and molten pool from atmospheric contamination. When welding thinner materials, edge joints, and flanges, welders generally do not use filler metals. However, for thicker materials, welders primarily use externally fed filler metal. TIG welding is a popular technique for joining thin materials in the manufacturing industries. This type of welding achieves a high quality weld for stainless steels and non-ferrous alloys. Compared with gas metal arc welding, the major limitations of TIG welding include its inferior joint penetration, its inability to weld thick materials in a single pass, and its poor tolerance to many material compositions, including cast-to-cast variations in the composition of certain impurities, as described by Fujii et al. (2008) and Huang (2009). The threshold for butt-joint penetration when welding stainless steel plates using a single pass TIG process is only 3 mm.

One approach to improve TIG penetration is to add small concentrations of active chemical elements, such as oxygen or sulfur, to the molten pool. The welding research can accomplish this by implementing a number of techniques. Fujii et al. (2008), Huang (2009), Leconte et al. (2006), Liu and Sun (2008), Xu et al. (2007), and Zhang et al. (2008) proposed one of the most notable techniques is to use an activated flux in TIG welding process. This novel variant of the TIG process is called activated TIG welding, which uses a thin layer of activated flux on the surface of the joint. The primary benefit of using flux is to reduce the heat energy required for TIG penetration. Researchers at the Paton Welding Institute in Ukraine

* Corresponding author. Tel.: +886 8 7703202; fax: +886 8 7740552.
E-mail address: tkh@mail.npust.edu.tw (K.-H. Tseng).

0924-0136/$ – see front matter © 2010 Elsevier B.V. All rights reserved.
doi:10.1016/j.jmatprotec.2010.11.003

Table 1
Nominal chemical composition (wt%, balance Fe) and mechanical properties of experimental duplex stainless steels.

C	Si	Mn	P	S	Cr	Ni	Mo	N	Tensile strength, MPa	Elongation, %
0.020	0.47	1.77	0.031	0.002	17.10	10.11	2.05	0.048	587	53

introduced the concept of using flux with TIG to increase joint penetration in the 1960s outlined by Gurevich et al. (1965). Sun and Pan (2004) reported that activated TIG welding can significantly increase penetration capability by as much as 300% compared with the conventional TIG welding.

The activated flux may have two types of mechanisms, one based on the Marangoni convection effect, and the other based on weld arc behavior. Heiple and Roper (1981, 1982) and Heiple et al. (1983) proposed surface active elements in the molten pool change the temperature coefficient of surface tension from negative to positive, thereby reversing the Marangoni convection direction from outward to inward. As the direction of the fluid flow in the molten pool becomes inward, the joint penetration increases dramatically. Lucas and Howse (1996) and Howse and Lucas (2000) associated the greater penetration of activated TIG welding to a constriction of the arc. However, due to limited data are available in literature about the action of weld arc and the mechanisms that sustain this effect, this phenomenon requires further investigation. Information on these processes is necessary to determine the TIG penetration capability improvement function of the activated flux. Because austenitic stainless steels have a higher coefficient of thermal expansion and lower thermal conductivity than carbon and alloy steel, it can induce a large amount of shrinkage and distortion after welding fabrication. Determining the effect of the activated flux on weld distortion is essential to improving the performance of the stainless steel activated TIG technique. This study used five different kinds of oxide fluxes to investigate the effect of single-component flux on the morphology and distortion of Type 316L stainless steel TIG welds. Aside from studying the microstructure and hardness of activated TIG weld metal, this study investigated the theoretical and experimental mechanisms for increasing the activated TIG penetration capability.

2. Experimental procedure

Type 316L stainless steel plate was selected as the test specimen. Table 1 lists the chemical compositions and mechanical properties of this steel. Plates 6 mm in thickness were cut into 150 × 130 mm strips, roughly polished with 400 grit silicon carbide paper to remove surface contamination, and then cleaned with acetone. Activated flux was prepared using five kinds of single component oxides (MnO_2, TiO_2, MoO_3, SiO_2, and Al_2O_3) packed in powdered form with about 30–60 μm particle size. These powders were mixed with acetone to produce a paint-like consistency. Before welding, a thin layer of the flux was brushed on to the surface of the joint to be welded. The coating density of flux was about 5–6 mg/cm^2. Fig. 1 shows a schematic diagram of activated TIG welding.

An autogenous TIG process was performed on the test specimen using an automatic welding machine to produce a bead-on-plate welded joint. A machine-mounted torch with a standard 2% thoriated tungsten electrode was used. The tip angle of electrode was ground and the electrode gap was measured for each weld before welding to ensure that the weld deposit was performed under the same conditions. Table 2 lists the standard welding conditions used in this study. During welding, a charge coupled device detector was used to observe and record images of the weld arc. To record the

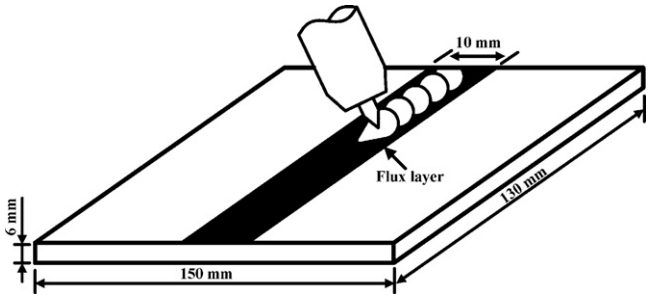

Fig. 1. Schematic diagram of activated TIG welding.

Table 2
Welding parameters for autogenous TIG welding experiments.

Weld current	200 A
Travel speed	150 mm/min
Diameter of electrode	3.2 mm
Tip angle of electrode	45°
Electrode gap	2 mm
Shielding gas	Pure argon
Gas flowrate	10 l/min

experimental conditions, a digital video recorder system continuously monitored the arc voltage.

After welding, experiments were carried out to measure the angular distortion in a bead-on-plate welded joint. The mean vertical displacement method measured the distortion, as Fig. 2a schematically illustrates. A hole was drilled at the back of points P_1, P_2, and P_3, and a pillar was inserted in each hole. Three pillars (one fixed, two adjustable) were used to adjust the horizontal level, and the distance from each point to the horizontal surface was then recorded. Measurements were taken before and after welding. The differences in measurements before and after welding revealed the

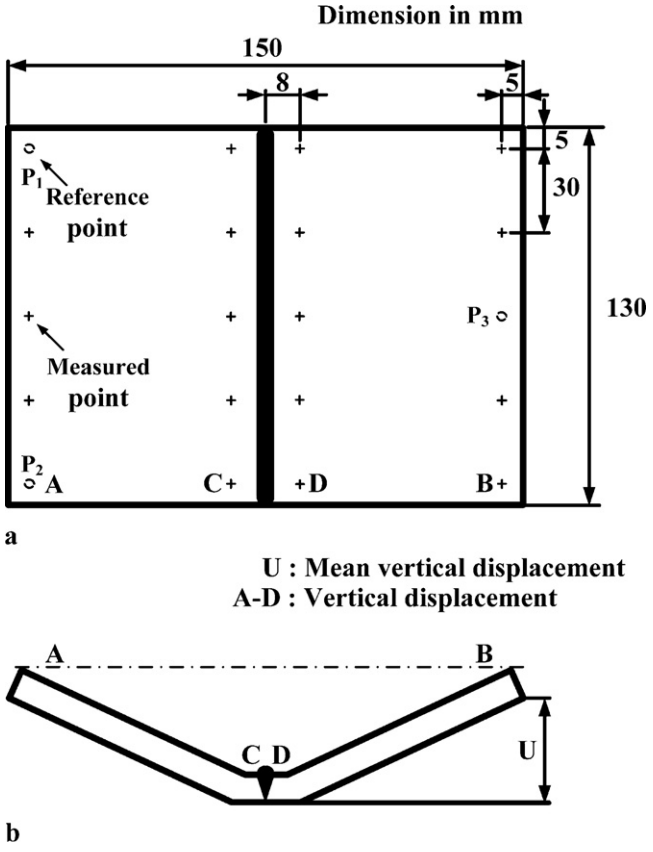

Fig. 2. Schematic diagram of distortion measurement.

a The conventional TIG electrode with diameter 2.4 mm

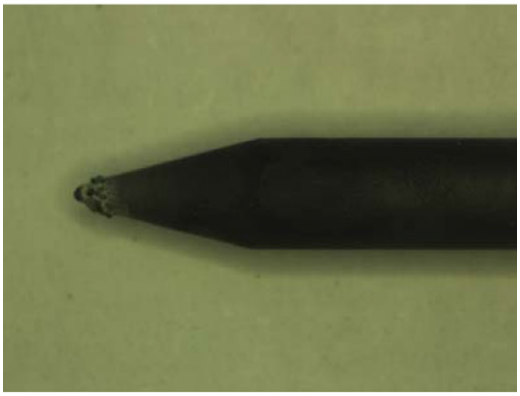

b The activated TIG electrode with diameter 2.4 mm

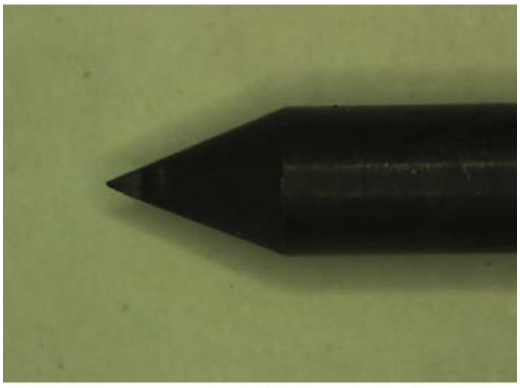

c The activated TIG electrode with diameter 3.2 mm

Fig. 3. Effect of activated flux on TIG electrode tip.

vertical displacement caused by welding, and the angular distortion value U can be derived from the equation

$$\left|U\right| = \frac{(A+B)-(C+D)}{2} \quad (1)$$

where A, B, C, and D represent the mean vertical displacement values of each point, as Fig. 2b shows.

The Fisher make ferritoscope was used for measuring the delta-ferrite content of the weld metal and base material. This device detects phases such as ferrite by their magnetic susceptibility, which differs from that of the paramagnetic austenite. To minimize measurement errors due to weld metal inhomogeneity, the average value of seven measurements from different locations along the welded surface was recorded.

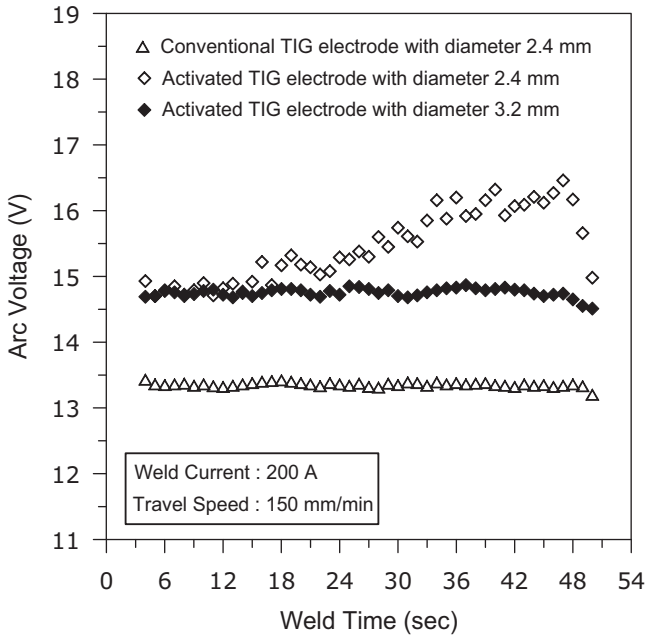

Fig. 4. Effect of activated flux and electrode diameter on arc voltage.

The microhardness test was used to examine the metallurgical properties of Type 316L stainless steel welds. The hardness profiles across the weld metal, heat-affected zone, and base material were measured under a load of 2.94 N for 15 s, and the position of the hardness test was 1 mm below the weld surface on the cross-section.

An optical microscope was used to measure the weld depth and bead width. All metallographic specimens were prepared using standard procedures, including mechanical lapping, grinding, and polishing to a 0.05 μm finish, followed by etching in a solution of 10 g $CuSO_4$–50 ml HCl–50 ml H_2O.

3. Results and discussion

3.1. Evaluation of the electrode tip

The evaluation experiment was performed using a direct current electrode negative TIG power supply. Bead-on-plate TIG welding was carried out with and without SiO_2 flux at electrode diameters of 2.4 and 3.2 mm. The experimental results in Fig. 3a clearly indicated no damage to the tip of the 2.4 mm electrode during TIG welding without flux. However, the 2.4 mm electrode tip melted seriously during TIG welding with SiO_2 flux (Fig. 3b) as a result of a higher heat input during activated TIG welding. Fig. 4 shows the effect of activated flux and electrode diameter on arc voltage. The weld current, travel speed, and electrode diameter were maintained at a constant value, and it was found that the arc voltage increases when activated TIG welding technique was used. Since the calculated heat input is proportional to the measured arc voltage, applied oxide flux has the positive effect of increasing the heat input in welding fabrication. The oxide fluxes are generally inorganic materials that act as high electric insulators. Experimental results indicated that the high heat load of the activated TIG electrode came from the heat reflected by the higher surface insulation resistance of the inorganic flux. When a small diameter electrode used for a high degree of weld heat led to overheating, the tungsten particles fell into the molten pool and contaminated the TIG weld metal. Fig. 3c shows an optimal tip configuration of the activated TIG electrode obtained using a 3.2 mm electrode.

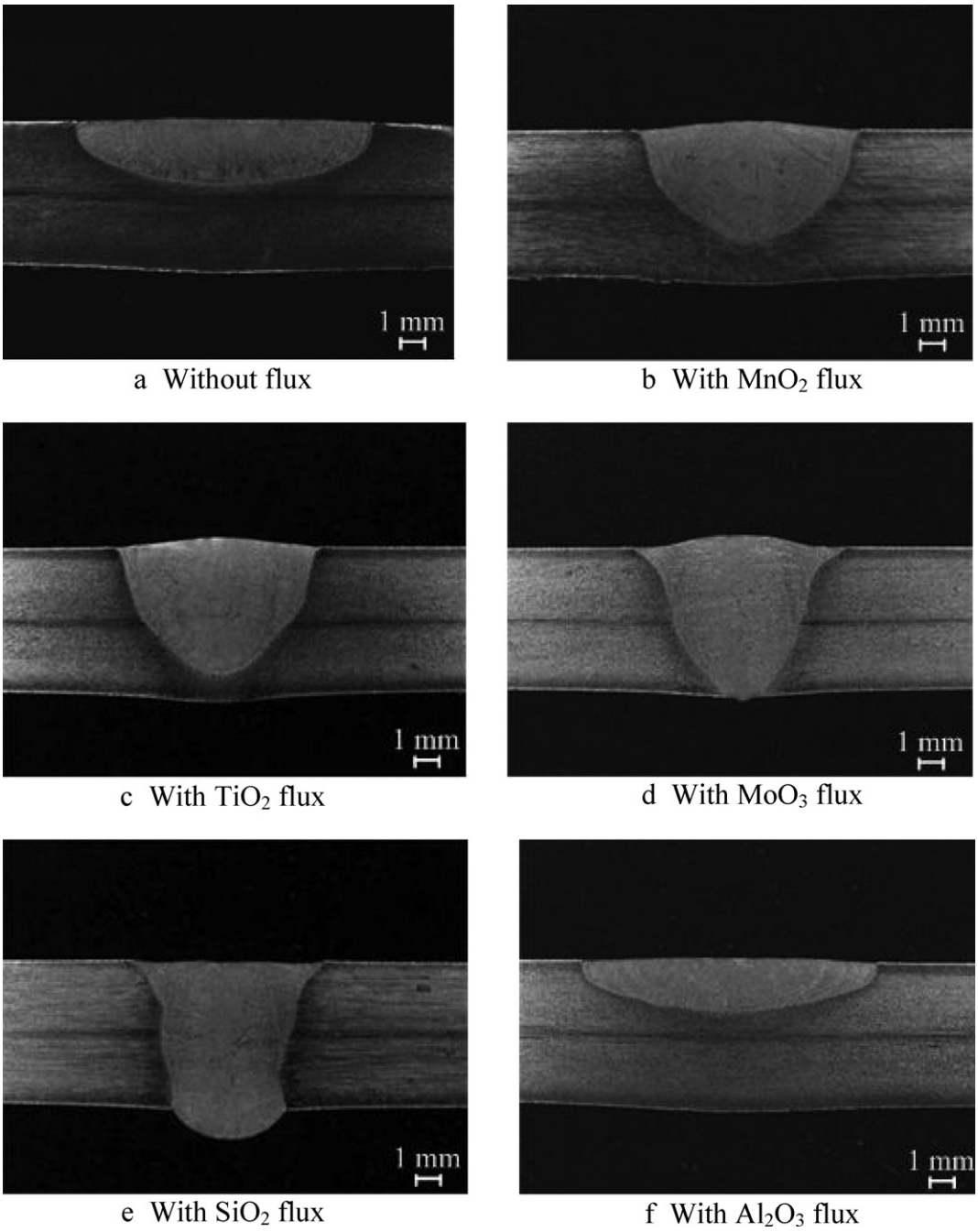

Fig. 5. Effect of activated flux on weld morphology.

Fig. 4 also shows that the activated TIG arc voltage produced by a 2.4 mm electrode exhibited an unstable state compared with a 3.2 mm electrode. TIG welding with flux greatly increased the magnitude of the welding heat input, causing much greater tip wear for the smaller electrode. In addition, the electrode gaps reveal variations in weld times, leading to arc instability during activated TIG welding. To obtain high quality welds and stable weld arc, the activated TIG welding requires large diameter electrodes to support a given level of the weld current. This is because the electrode tip is not cooled by the thermal emission of electrons but by their impact.

3.2. *Effect of oxide flux on weld morphology*

According to work by Heiple and Roper (1981, 1982) and Heiple et al. (1983), the direction of fluid flow in the molten pool can affect the weld morphology. The temperature coefficient of surface tension is a factor in driving the direction of fluid flow in the molten pool. Fig. 5 shows the morphology of TIG welds in 6 mm thick Type 316L stainless steels, with and without flux. During welding, it is always a difficult task to measure the temperature of the molten pool since this region is surrounded by hot plasma. However, it is well known that the temperature gradient always exists on the surface of the TIG molten pool, accompanied by higher temperatures in the pool center under the arc, and lower temperatures at the pool edge.

When using TIG welding without flux, the temperature coefficient of surface tension on the molten pool generally exhibited a negative value. If the surface tension in the pool center is lower than the temperature at the pool edge, then the surface tension gradient $d\sigma/dT$ generates centrifugal Marangoni convection in the

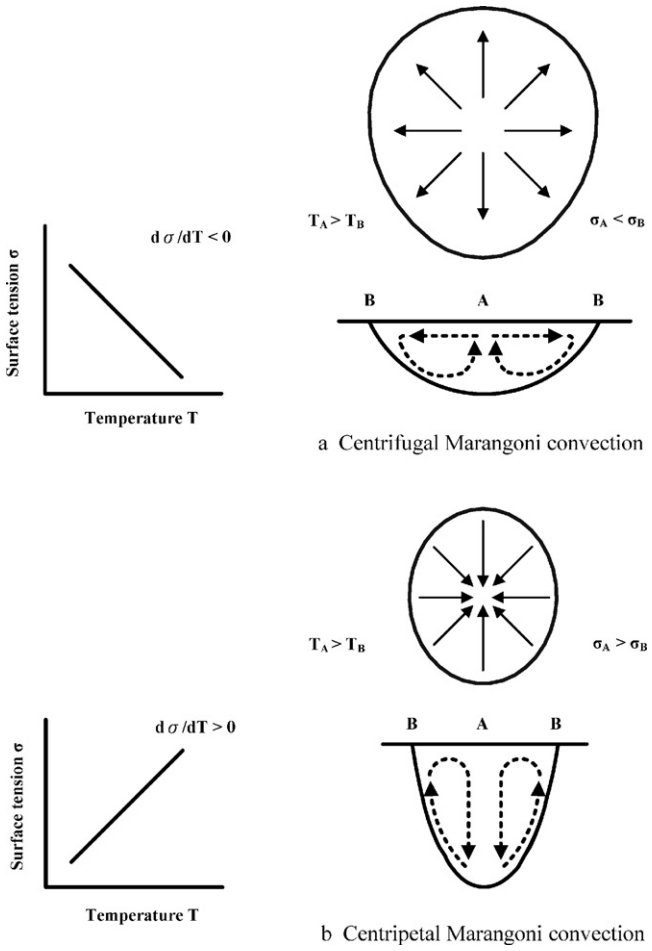

Fig. 6. Schematic diagram of Marangoni convection mode.

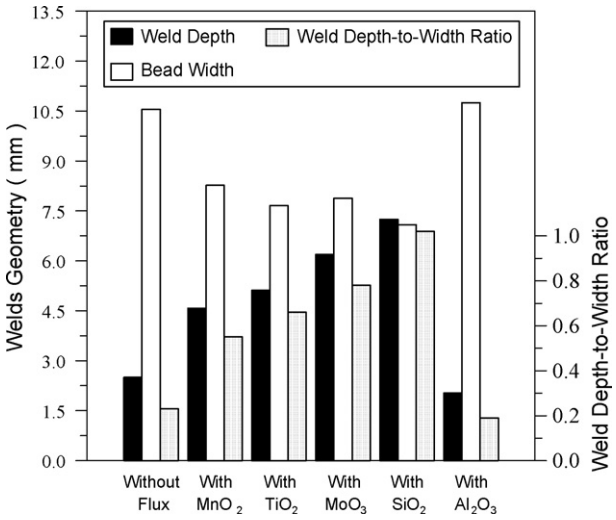

Fig. 7. Characteristics of weld geometry produced with and without flux.

molten pool (Fig. 6a). In this condition, the fluid flow of the molten pool surface transfers easily from the pool center to the edge, yielding a wide and shallow TIG weld (Fig. 5a). When TIG welding with MnO_2, TiO_2, MoO_3, and SiO_2 fluxes is used, the temperature coefficient of surface tension on the molten pool changed from a negative to a positive value. Therefore, the surface tension at the pool center was higher than at the pool edge. This indicated that the surface tension gradient introduces centripetal Marangoni convection in the molten pool (Fig. 6b). In this condition, the fluid flow of the molten pool surface easily transfers from the pool edge to the center, and then downward. Fig. 5b–e shows that this results in a narrow and deep TIG weld that forms a peanut shell-like shape. This result showed that using SiO_2 and MoO_3 fluxes created a significant increase in weld depth and a decrease in bead width. The SiO_2 flux can facilitate root pass joint penetration of Type 316L stainless steel. Fig. 5f shows that the Al_2O_3 flux has a negative effect on the activated TIG weld morphology. Not all oxide fluxes can change the Marangoni convection mode by altering the temperature coefficient of surface tension.

Fig. 7 shows the characteristics of the Type 316L stainless steel TIG weld geometry produced with and without flux. Using MnO_2, TiO_2, MoO_3, and SiO_2 fluxes produced a significant increase in weld depth and a decrease in dead width, with Al_2O_3 flux being the major exception. The experimental results also showed that the MnO_2, TiO_2, MoO_3, and SiO_2 fluxes provided a high weld depth-to-width aspect ratio.

This study applied Simonik (1976) principle of electron absorption to account for the observed arc constriction and the increased joint penetration. The cross-sectional view of an arc column normally appears round, as it consists of two concentric zones. These zones include an inner core and an outer region. The inner core of the arc carries the majority of the current, and has the highest temperature. The outer region of the arc is much cooler, and tends to keep the arc plasma within the central region. For arcing with and without flux, the glowing zone in Fig. 8 shows that the inner core of the arc occupies almost the entire arc length. This zone is the arc column. Fig. 8 shows that activated TIG welding constricts the arc column compared to a conventional TIG arc at the same current level. In the inner core of the arc, the plasma temperature is higher than the dissociation temperature of the ionic flux and shielding gas. In addition, ionizing the atoms and molecules generates positive ions and electrons. In the outer region of the arc, however, the dissolved flux still exists as atoms or molecules large enough for the electrons to attach to form negative charges. This reduces the number of electrons in the outer region of the arc (the major charge carriers), which constricts the diameter of arc column. Physically constricting the arc column can improve the concentration of heat energy in the anode root (Huang et al., 2005), and achieve a greater aspect ratio of the activated TIG welds compared with conventional TIG welds.

On the basis of the present results, it is considered that the surface tension gradient and plasma arc column play a role in increasing the penetration of activated TIG joint. Due to the presence of oxygen in the oxide flux, the temperature coefficient of surface tension on the molten pool changed from the negative to the positive, which caused centripetal Marangoni convection mode. Corresponding heat transfer from the weld surface to the root caused the metal plasma to be localized at the center of the molten pool. As a result, a constricted anode root was formed, and higher current density and energy concentration in the arc column further promoted the centripetal Marangoni convection in the molten pool driven by Lorentz force (Chern et al., 2011), which in turn brought about a greater arc forces acting on the molten pool. Therefore, the multiplied effect of the centripetal Marangoni convection and constricted arc plasma will not only produce a narrower bead width but also increase the weld depth when using activated TIG welding. Although further investigation must clarify the physical mechanisms involved in this phenomenon, this study demonstrated the effect of specific flux on the activated TIG welds.

Fig. 9 depicts the surface of Type 316L stainless steel TIG welds with Al_2O flux, showing excessive residual slag floating on both sides of the welded surface. However, this no residual slag appeared

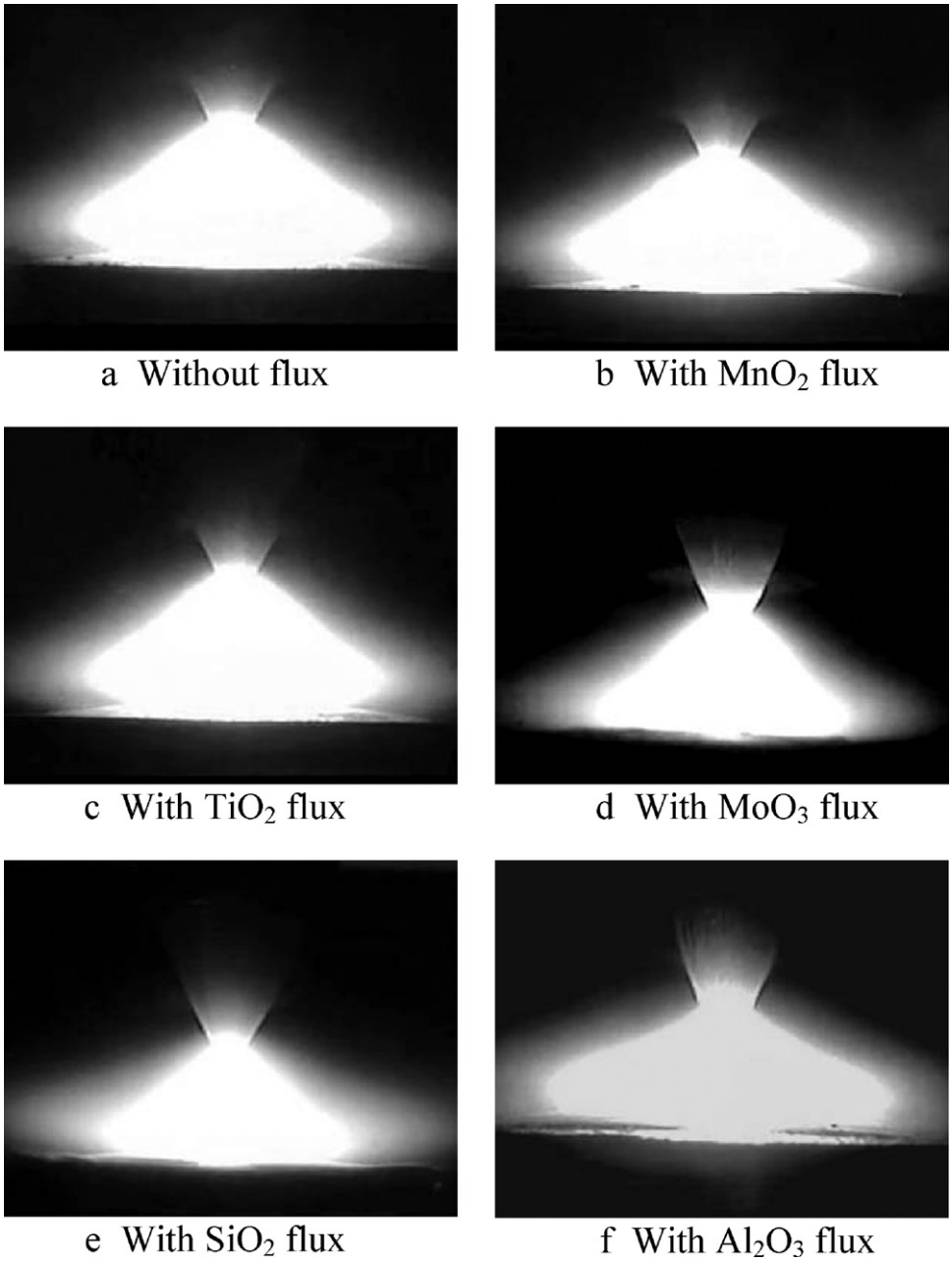

Fig. 8. Effect of activated flux on weld arc.

in the central region of the welded surface. Fig. 10 schematically shows the Marangoni convection mode for aluminum oxide particles. Because TIG welding with Al_2O_3 flux produces a radially outward flow from the pool center, an aluminum oxide particle-free band forms along the pool edge. This fluid flow in the molten pool surface easily transfers heat to the pool edge, producing wider and shallower welds compared with conventional TIG welding (Fig. 5f). TIG welding with aluminum oxide flux appears unable to constrict the arc column (Fig. 8f). This result may be related to the thermodynamic stability of aluminum oxide. According to the Ellingham diagram, which plots the Gibbs free energy change in oxidation reaction versus temperature, aluminum oxide has a high degree of thermodynamic stability. Since the temperature of the outer region of the arc may be lower than the dissociation temperature of the Al_2O_3 flux, aluminum oxide is particularly difficult to dissolve. Therefore, there is no reduction in the number of electrons in the cooler outer region of the arc, and no constriction of the arc column. This situation causes an aluminum oxide particle-free band to be formed along the edge of the molten pool, producing excessive residual slag on both sides of the welded surface.

3.3. *Effect of oxide flux on angular distortion*

The distortion of the weldment is a result of the expansion and contraction of the weld metal and the adjacent base material during welding thermal cycle. Uneven heating through the thickness of a joint plate during welding causes non-uniform transverse shrinkage, yielding angular distortion of the weldment. Fig. 11 shows the effects of TIG welding on the angular distortion of Type 316L stainless steel welding with and without flux. It was clearly identified that activated TIG welding reduces the measured angular distortion of the weldment.

For TIG welding with Al_2O_3 flux, the weld depth is not more than the half of plate thickness. The shallow weld depth causes

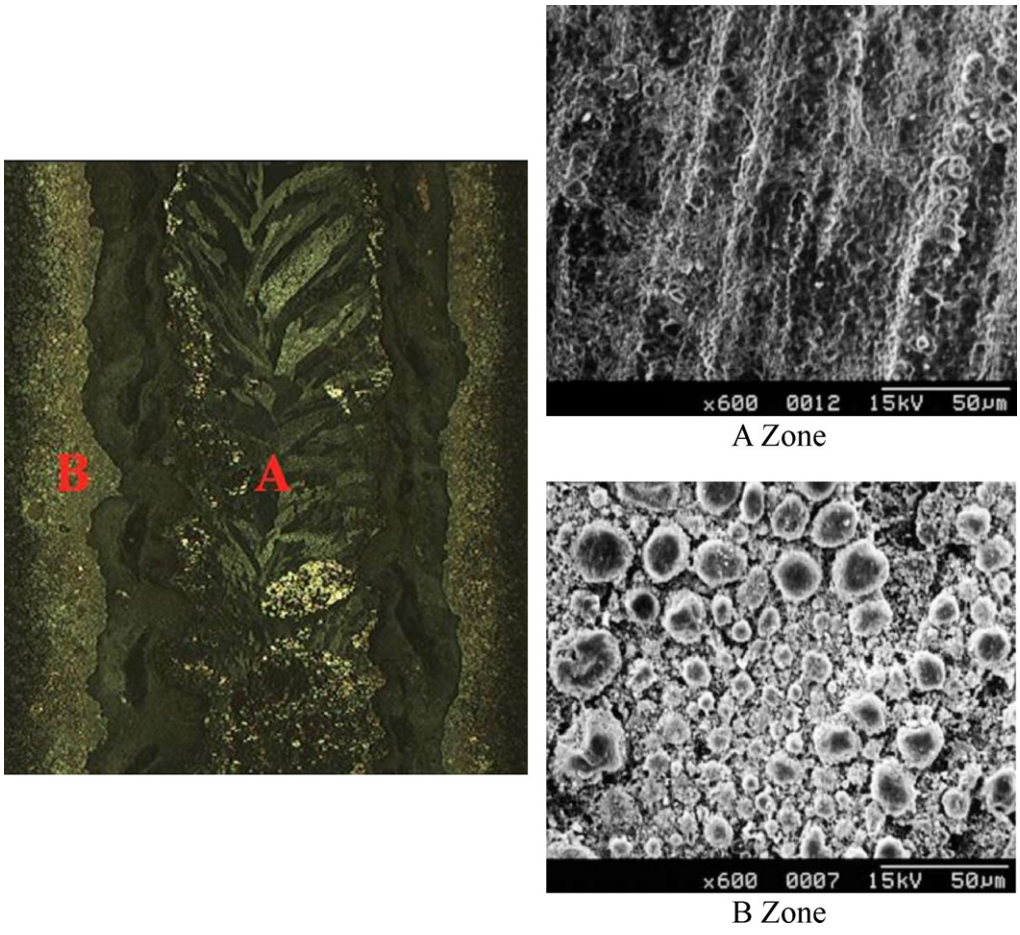

Fig. 9. Effect of Al_2O_3 flux on weld surface appearance.

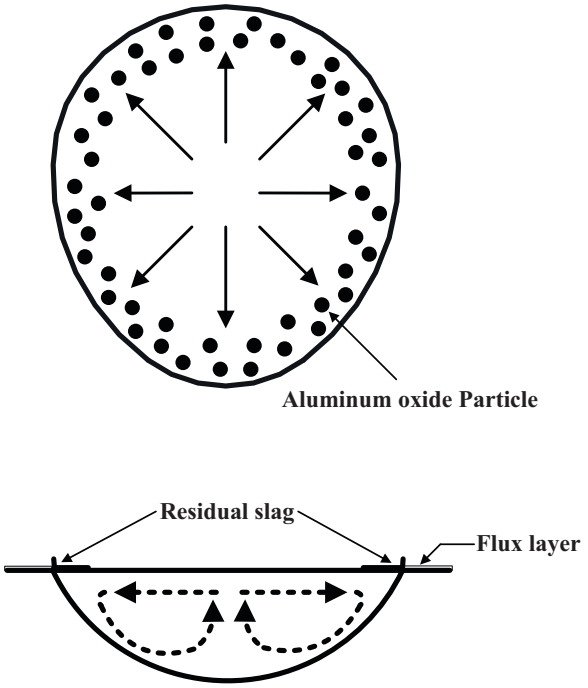

Fig. 10. Schematic diagram of Marangoni convection for aluminum oxide particles.

lower angular distortion, and with increasing weld depth to plate thickness ratio, the angular distortion of the weldment without flux increases to a critical point (weld depth to plate thickness ratio equivalent to 0.5), and then weld depth exceeds 50% of the

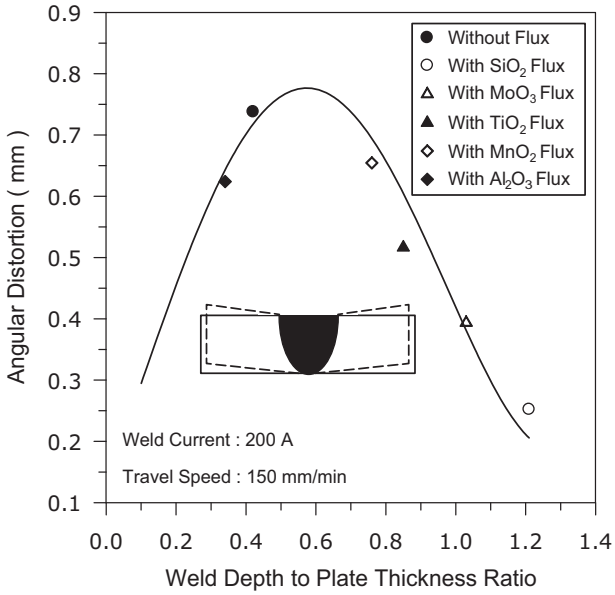

Fig. 11. Effect of activated flux on angular distortion of the weldment.

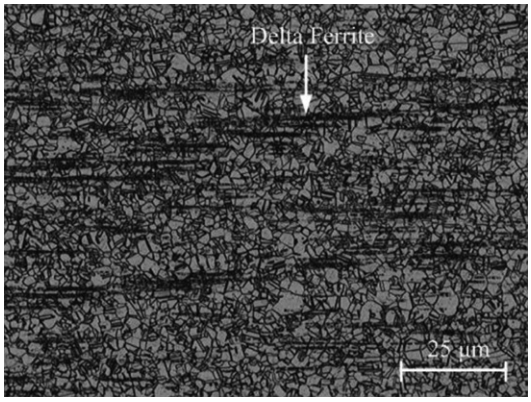

Fig. 12. Optical micrograph of Type 316L stainless steel base metal.

plate thickness, the angular distortion of the weldment with use of the MnO_2, TiO_2, MoO_3, and SiO_2 fluxes decreases. Activated TIG welding increases both the joint penetration and the weld depth-to-width ratio, which indicates a high degree of energy concentration during activated TIG welding. This contributes to a reduction in the quantity of supplied heat, which prevents overheating of the base material and reduces the incidence of thermal stress and incompatible strain due to shrinkage in thickness. Therefore, the activated TIG welding can significantly reduce the angular distortion of the weldment. The variations in angular distortion correlate to a weld depth relative to the plate thickness, and the shape and dimensions of the welds (Pavlovsky and Masubuchi, 1994; Tseng and Chou, 2001, 2003). In addition, full penetration and a large weld depth-to-width ratio result in the lowest angular distortion. This result showed that Type 316L stainless steel TIG welding with SiO_2 flux produced a substantial increase in the weld depth and weld depth-to-width ratio of about 7.25 mm and 1.02,

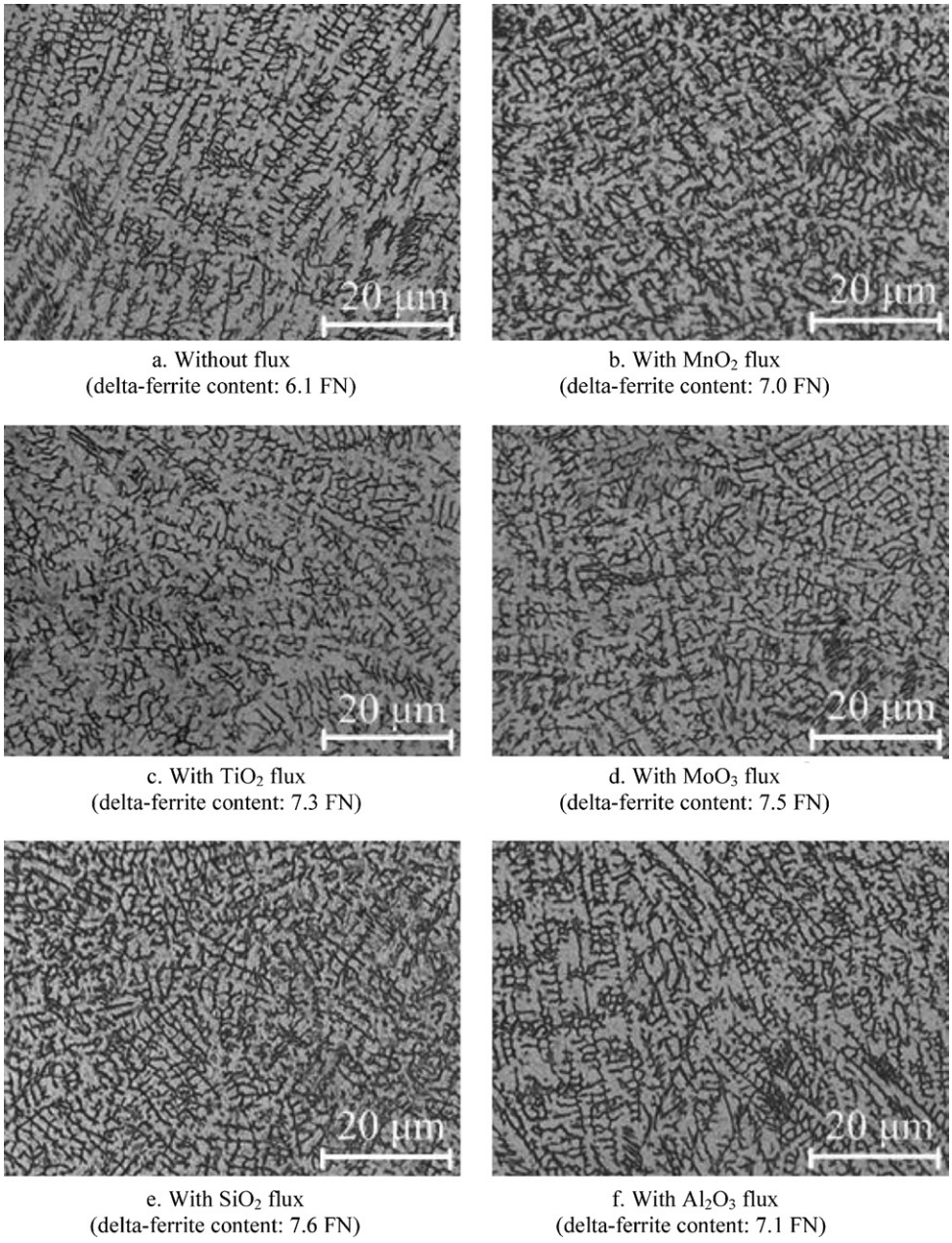

a. Without flux (delta-ferrite content: 6.1 FN)

b. With MnO_2 flux (delta-ferrite content: 7.0 FN)

c. With TiO_2 flux (delta-ferrite content: 7.3 FN)

d. With MoO_3 flux (delta-ferrite content: 7.5 FN)

e. With SiO_2 flux (delta-ferrite content: 7.6 FN)

f. With Al_2O_3 flux (delta-ferrite content: 7.1 FN)

Fig. 13. Effect of activated flux on microstructures and delta-ferrite content.

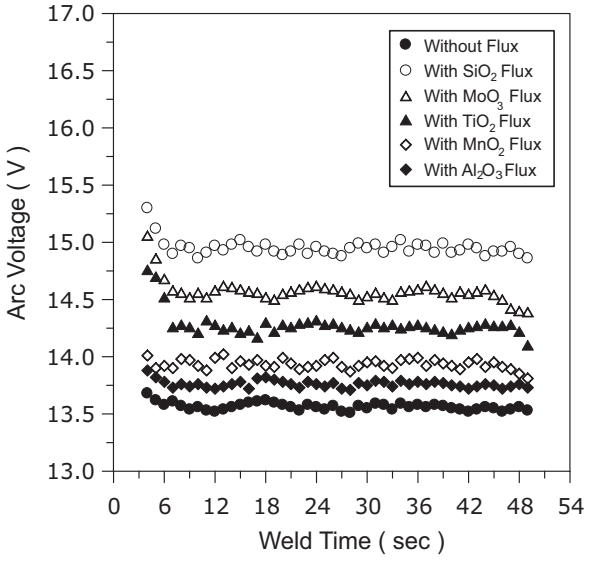

Fig. 14. Effect of activated flux on arc voltage.

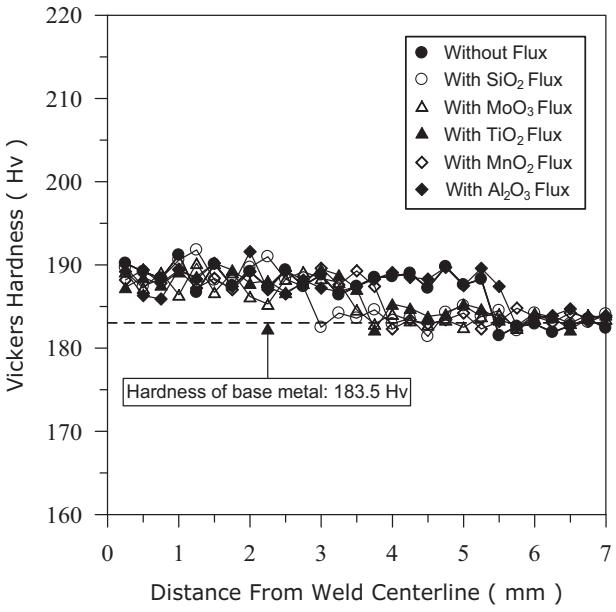

Fig. 15. Effect of activated flux on hardness profile of the weldment.

respectively. TIG welding with SiO_2 flux heated the base metal more evenly throughout its thickness, significantly reducing the angular distortion of the weldment.

3.4. Effect of oxide flux on microstructure and hardness

The experiments used Type 316L hot rolled stainless steel plate as a base metal. The ferrite number (FN) was measured using a calibrating magnetic instrument with a FERITSCOPE FMP30. Fig. 12 shows the microstructure of Type 316L stainless steel base metal with an average of 1.2 FN delta-ferrite content in an austenite matrix. This result also indicated that the stringers of delta-ferrite elongate in the rolling direction. Fig. 13 shows the microstructure and measured delta-ferrite content in Type 316L stainless steel weld metal produced with and without flux. In Type 316L stainless steel TIG welds produced without flux, the delta-ferrite content increased to 6.1 FN from its initial value of 1.2 FN. This is because most of the weld metal of austenitic stainless steel solidified as delta-ferrite phase. During welding, the cooling rate of the weld metal was so rapid that the phase transformation of delta-ferrite to austenite did not complete. Consequently, more delta-ferrite retained in the weld metal after solidification. On the other hand, when using oxide fluxes, the delta-ferrite content in activated TIG weld metal slightly increased to 7.0–7.6 FN. This result is related to the heat input during TIG welding with and without flux. The effect of TIG welding with and without flux on the arc voltage is shown in Fig. 14. The weld current was maintained at constant value, and it was found that the arc voltage increases when the activated TIG process was used. Since the calculated heat input is proportional to the measured arc voltage, applied activated flux has the positive effect of increasing the heat input unit length of welds. Because this higher heat input can increase the peak temperature of the welds, and consequently, more delta-ferrite forms in the activated TIG weld metal. All cases exhibited a microstructure of austenite matrix and vermicular delta-ferrite morphology typical of this class of material. However, there were no major differences between the microstructure of the conventional TIG and the activated TIG weld metal.

Fig. 15 presents the experimental results for the hardness profile of the TIG weldment with and without flux. The results showed that the oxide flux did not produce a significant change the hardness of Type 316L stainless steel weld metal. The austenite has a cubic face-centered (FCC) crystal structure. The delta-ferrite has a body-centered cubic (BCC) crystal structure. The BCC structure has a higher mechanical strength than that of the FCC structure. When TIG welding with or without flux is used, the delta-ferrite content in the weld metals is increased, and has a beneficial effect in increasing the hardness of Type 316L stainless steel welds.

4. Conclusions

This paper conducted detailed experiments to systematically investigate the effect of MnO_2, TiO_2, MoO_3, SiO_2, and Al_2O_3 fluxes on weld morphology, angular distortion, delta-ferrite content, and hardness when using the TIG process to weld 6 mm thick Type 316L stainless steel plates. The primary results and conclusions are summarized as follows:

1. To obtain high quality welds and stable weld arc, the activated TIG process requires large diameter electrodes to support a given level of the weld current.
2. TIG welding with SiO_2 and MoO_3 fluxes achieves an increase in weld depth and a decrease in bead width, respectively. The SiO_2 flux can facilitate root pass joint penetration, but the Al_2O_3 flux led to a deterioration in the penetration compared to the conventional TIG process for Type 316L stainless steel welds.
3. The interaction between the centripetal Marangoni convection and the constricted arc plasma as a mechanism in increasing activated TIG penetration.
4. Activated TIG welding can increase the joint penetration and weld depth-to-width ratio, significantly reducing the angular distortion of the weldment.
5. Since the activated TIG welding can increase the arc voltage, the amount of heat input per unit length in a weld is also increased, and therefore the delta-ferrite content in weld metal will be increased. The addition of oxide flux does not significantly affect the hardness of Type 316L stainless steel activated TIG weld metal.

Acknowledgements

The authors gratefully acknowledge the financial support for this research provided by the National Science Council, Taiwan, Republic of China, under Grant No. NSC 98-2221-E-020-015.

References

Chern, T.S., Tseng, K.H., Tsai, H.L., 2011. Study of the characteristics of duplex stainless steel activated tungsten inert gas welds. Mater. Des. 32 (1), 255–263.

Fujii, H., Sato, T., Lu, S.P., Nogi, K., 2008. Development of an advanced A-TIG (AA-TIG) welding method by control of Marangoni convection. Mater. Sci. Eng. A 495, 296–303.

Gurevich, S.M., Zamkov, V.N., Kushnirenko, N.A., 1965. Improving the penetration of titanium alloys when they are welded by argon tungsten arc process. Avtom. Svarka. 9, 1–4.

Heiple, C.R., Roper, J.R., 1981. Effect of selenium on GTAW fusion zone geometry. Weld. J. 60 (8), 143s–145s.

Heiple, C.R., Roper, J.R., 1982. Mechanism for minor element effect on GTA fusion zone geometry. Weld. J. 61 (4), 97s–102s.

Heiple, C.R., Roper, J.R., Stagner, R.T., Aden, R.J., 1983. Surface active element effects on the shape of GTA. Laser, and electron beam welds. Weld. J. 62 (3), 72s–77s.

Howse, D.S., Lucas, W., 2000. Investigation into arc constriction by active fluxes for tungsten inert gas welding. Sci. Technol. Weld. Join. 5 (3), 189–193.

Huang, H.Y., 2009. Effects of shielding gas composition and activating flux on GTAW weldments. Mater. Des. 30 (7), 2404–2409.

Huang, H.Y., Shyu, S.W., Tseng, K.H., Chou, C.P., 2005. Evaluation of TIG flux welding on the characteristics of stainless steel. Sci. Technol. Weld. Join. 10 (5), 566–573.

Leconte, S., Paillard, P., Chapelle, P., Henrion, G., Saindrenan, J., 2006. Effect of oxide fluxes on activation mechanisms of tungsten inert gas process. Sci. Technol. Weld. Join. 11 (4), 389–397.

Liu, L., Sun, H., 2008. Study of flux assisted TIG welding of magnesium alloy with SiC particles in flux. Mater. Res. Innov. 12 (1), 47–51.

Lucas, W., Howse, D., 1996. Activating flux – increasing the performance and productivity of the TIG and plasma processes. Weld. Met. Fab. 64 (1), 11–17.

Pavlovsky, V.I., Masubuchi, K., 1994. Research in the USSR on residual stresses and distortion in welded structures. Weld. Res. Counc. Bull. 388, 44–48.

Simonik, A.G., 1976. The effect of contraction of the arc discharge upon the introduction of electro-negative elements. Weld. Prod. 3, 49–51.

Tseng, K.H., Chou, C.P., 2001. Effect of pulsed gas tungsten arc welding on angular distortion in austenitic stainless steel weldments. Sci. Technol. Weld. Join. 6 (3), 149–153.

Tseng, K.H., Chou, C.P., 2002a. Effect of nitrogen addition to shielding gas on residual stress of stainless steel weldments. Sci. Technol. Weld. Join. 7 (1), 57–62.

Tseng, K.H., Chou, C.P., 2002b. The effect of pulsed GTA welding on the residual stress of a stainless steel weldment. J. Mater. Proc. Technol. 123, 346–353.

Tseng, K.H., Chou, C.P., 2003. The study of nitrogen in argon gas on the angular distortion of austenitic stainless steel weldments. J. Mater. Proc. Technol. 142, 139–144.

Xu, Y.L., Dong, Z.B., Wei, Y.H., Yang, C.L., 2007. Marangoni convection and weld shape variation in A-TIG welding process. Theor. Appl. Fract. Mec. 48, 178–186.

Sun, Z., Pan, D., 2004. Welding of titanium alloys with activating flux. Sci. Technol. Weld. Join. 9 (4), 337–344.

Zhang, Z.D., Liu, L.M., Shen, Y., Wang, L., 2008. Mechanical properties and microstructures of a magnesium alloy gas tungsten arc welded with a cadmium chloride flux. Mater. Charact. 59, 40–46.